Building Next Generation In Vitro Models of the Renal Nephron at Anatomical Scale

Andres Armenta

A thesis

submitted in partial fulfillment of the

Requirements for the degree of

Master of Science

University of Washington

2026

Committee:

Ying Zheng

Joshua Vaughan

Program Authorized to Offer Degree:

Bioengineering

University of Washington

Abstract

Building Next Generation In Vitro Models of the Renal Nephron at Anatomical Scale

Andres Armenta

Chair of the Supervisory Committee:

Ying Zheng

Department of Bioengineering

Current biofabrication techniques for tissue engineering applications remain limited in their ability to produce perfusable structures with physiologically relevant dimensions, complex 3D organization, and anatomical geometry. In this work, we use multiphoton laser ablation of collagen hydrogels as a subtractive biofabrication strategy to create anatomical renal nephron microstructures, with a particular focus on proximal tubule architecture. To accomplish this, kidney imaging datasets were converted into ablation-compatible 3D models and fabricated within collagen microfluidic platforms. The resulting microchannels supported endothelial and epithelial cell culture and enabled reconstruction of anatomical nephron microenvironments in vitro. Furthermore, laser ablation enabled the fabrication of engineered proximal tubule microchannels with both controlled 3D curvature and luminal diameters below 100 μm, which remains difficult to achieve using conventional biofabrication approaches. Lastly, using these

engineered tubular microenvironments, we investigated human renal epithelial cell organization within anatomically scaled lumens. Overall this work extends multiphoton laser ablation from vascular microstructure fabrication towards epithelial nephron engineering, and establishes a versatile approach for generating anatomically organized microscale tissue architecture within collagen hydrogels.

Table of Contents

List of Figures

Acknowledgements

This work was supported financially by NIH grants 1U2CTR004867-01 and UG3 TR003288 awarded to Jonathan Himmelfarb, Edward Kelly, and Ying Zheng. The research collaboration of Jonathan Himmelfarb, Edward Kelly, and Joshua Vaughan is gratefully acknowledged. Andres Armenta's graduate studies were supported by the Northwest Comprehensive Research Training in Kidney, Urology, and Hematology (NCOR-KUH) TL1 program. The experimental support of Anish Mahadeo and Chetan Poudel is gratefully acknowledged.

1 | Introduction

Engineering physiologically relevant human tissues in vitro requires fabrication approaches capable of recreating the microscale geometry, three-dimensional organization, and extracellular matrix (ECM) environment of native tissues. In the kidney, nephron function depends on highly specialized microarchitectures spanning multiple length scales. For instance, the glomerulus, consists of a densely organized capillary network enclosed within the Bowman's capsule for blood filtration, while the proximal tubule consists of highly convoluted epithelialized microtubules that support selective reabsorption and solute transport. Additionally, the small scale of glomerular capillaries and proximal tubules leads to demanding requirements for biofabrication resolution. Specifically, biofabrication approaches need to be able to produce capillaries as small as 10 μm in diameter and tubules 40-60 μm in diameter without compromising the ability to organize tissues in 3D space. Accurately replicating glomerular and proximal tubule microstructure in vitro is necessary for mimicking the structural and hemodynamic cues experienced by renal cells in vivo. Therefore, developing a biofabrication strategy capable of reconstructing anatomical features in vitro may improve the physiologic relevance of engineered kidney models for disease modeling, drug screening, and regenerative medicine.

Various fabrication approaches, including soft lithography, sacrificial molding, extrusion bioprinting, and self-assembled organoids have been used to create renal tissues in vitro. Glomerulus models are commonly made with traditional microfluidics that allow for the culture of endothelial cells in a perfusable channel environment on permeable membranes [1]. These platforms are the current standard for in vitro glomerular modeling, allowing for endothelial-podocyte coculture and simulation of filtration across permeable surfaces. However,

microfluidic models currently lack the luminal architecture, scale, and branching complexity of glomerular capillary networks [2]. In order to bypass the difficulties of direct glomerular fabrication, previous studies have instead isolated glomeruli and subjected them to fluid flow inside of microfluidic traps [3]. Although glomerular microtissues were successfully isolated, glomeruli eventually lost structural integrity after onset of dynamic flow. Overall, there is a fundamental need for biofabrication strategies with the capacity of creating perfusable capillary networks with complex 3D morphologies in order to replicate glomerular structure in vitro. Recently, sacrificial gallium molding has been used to create multiscale vascular networks with complex biological forms [4]. This work has significantly advanced our ability to create perfusable vascular networks with branching architectures. However, it still remains difficult to produce perfusable vasculature at a capillary scale (>10 μm) and precise anatomical morphologies of glomerular capillaries have yet to be incorporated into any glomerular models.

Perfusable proximal tubule in vitro models were created as an improvement to 2D monolayer cultures and were first established within traditional microfluidic platforms [5]. These microfluidic models have provided the gold standard for in vitro analysis of proximal tubule epithelial cell metabolism and transport. More recently, extrusion bioprinting has been used to introduce tubule convolution and create models of the proximal tubule with 3D curvature. In particular, Homan et al. showed that perfusable, convoluted proximal tubule tissues can be fabricated by printing sacrificial pluronic ink in a gelatin-fibrinogen matrix [6]. This work established an important benchmark for the production of in vitro renal tubules with complex 3D morphologies. Similarly, van Genderen et al. showed an alternative coaxial printing approach that enabled fabrication of perfusable spiral tubule structures [7]. Although extrusion bioprinting has been successful in producing convoluted tubule models, the resolution of bioprinting

techniques remains larger than 100 μm and precise anatomical tubule structure has not yet been integrated into fabrication methodologies [8], [9]. The use of organoids has also been used in creating glomerular and tubular tissues in vitro. However, organoid models rely on cellular self assembly which results in large batch variability, no control over tissue structure, and cannot support controlled perfusion of created tissues [10]. Despite these advances, existing biofabrication methods remain limited in their ability to simultaneously achieve anatomical-scale luminal diameters, perfusability, 3D curvature, ECM compatibility, and direct conversion of imaging derived structures into engineered tissues for more physiological relevant modeling.

Multiphoton laser ablation has emerged as a promising subtractive biofabrication technique capable of patterning biomaterials with high spatial precision and full three-dimensional control. By focusing ultrashort laser pulses within a hydrogel volume, localized multiphoton absorption induces highly confined material removal at the focal point, enabling fabrication of enclosed microscale void spaces within native or synthetic biomaterials [11]. Previous studies of our group have demonstrated the ability of multiphoton ablation to create capillary-scale vascular geometries, guide endothelial cell migration, and fabricate organ-specific microvascular structures within collagen hydrogels [12], [13]. In addition, anatomically informed glomerular vascular models derived from imaging and computational reconstruction have demonstrated the importance of native geometry for glomerular hemodynamics and flow distribution [14]. However, extension of these subtractive biofabrication approaches toward epithelial nephron compartments, particularly anatomically tortuous proximal tubule structures at physiological microscale dimensions, has remained largely unexplored.

Here, we build on prior multiphoton ablation approaches for vascular and glomerular microstructure fabrication by extending this subtractive biofabrication strategy toward epithelial

nephron engineering. We combine kidney imaging-derived anatomical data with laser ablation of collagen hydrogels to create anatomically organized in vitro glomerular and proximal tubular microstructures within microfluidic platforms. In particular, we focus on proximal tubule architectures, where current biofabrication methods remain limited in producing both three-dimensional tortuosity and sub-100 μm luminal dimensions. By enabling epithelial cell culture within anatomically scaled tubular microenvironments, this work advances multiphoton laser ablation as a versatile approach for engineering microscale nephron structures in extracellular matrix hydrogels.

2 | Materials and Methods

2.1 | Kidney imaging data conversion into CAD files compatible for two-photon ablation

Laser ablation of anatomical structures relies on imaging and segmentation of tissue samples to produce three dimensional reconstructions that can be degraded into a material. Previously published glomerular reconstructions from mouse kidney serial sectioning and electron microscopy imaging were obtained as .obj files [15]. One reconstructed glomerulus composed of 89110 faces with intact afferent and efferent arterioles was selected and opened in Fusion 360, Autodesk for processing. The glomerulus structure was scaled by a factor of 1.5 and extensions were added to the arterioles to enable connection to pre-patterned microchannel networks. To facilitate ablation, the modified glomerulus was split into top and bottom halves which were abated in separate microscope scanning runs. The top and bottom glomerulus structures were then exported as .stl files and sliced into 1 μm thick layers in Netfabb, Autodesk. A total of 226 slices were then exported as vector graphics and converted into a .mdb file using a custom R script. The .mdb file was then imported into the Fluoview, Olympus software directing microscope scanning (Figure 1A).

Proximal tubule Z-stack segmentations were obtained as binary masks from reactive fluorophore stained mouse kidney tissue and expansion microscopy [16]. The binary masks were eroded in FIJI, locations of improper tubule connection were separated with the paintbrush tool, and masks were eroded again. The 3D viewer plugin in FIJI was then used to reconstruct the binary mask into a 3D object by visualizing it as a surface and exporting it as an .obj file. The reconstructed renal tubule was then visualized in Meshlab and the proximal tubule was isolated by trimming

before the clear narrowing of the loop of henle. Any remaining structural artifacts such as improper connections or separated surfaces were removed in Meshlab by deleting artifact vertices and running the close holes function. After this, duplicate vertices were removed and several iterations of uniform mesh resampling and HC laplacian smoothing were conducted to yield a final mesh composed of 658136 faces. The processed mesh was exported as an .stl file, repaired in Fusion 360 with stitching and defect removal, and converted into a solid body. Lastly, a 350 μm long segment was isolated from the complete proximal tubule structure and extensions were added for connection to pre-patterned microchannel networks. The proximal tubule segment CAD object was sliced into 205 individual slices and converted into a vector graphical representation using the same procedure previously described for the glomerulus (Figure 1B).

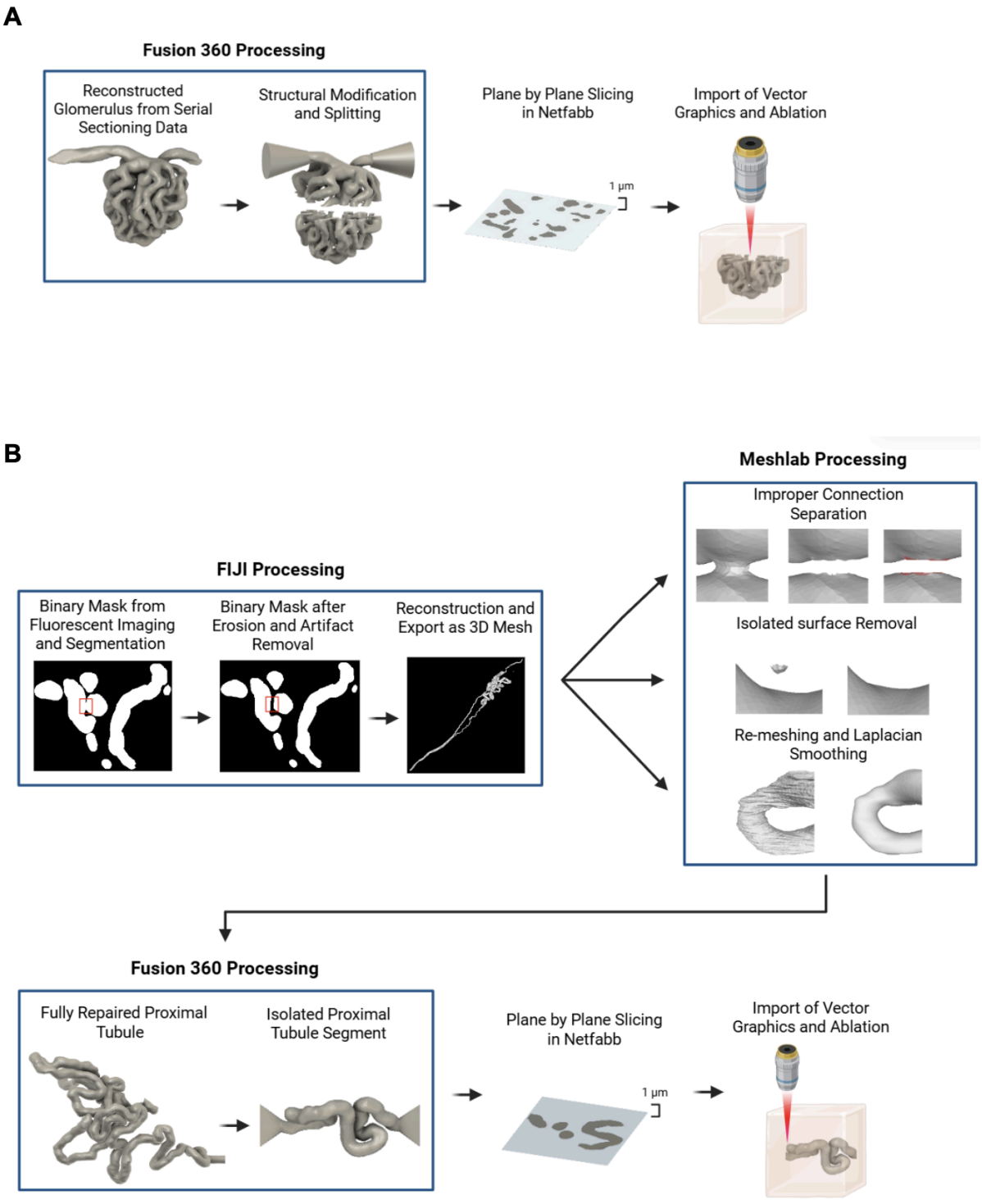

Figure 1: Generalized process for creating ablation-compatible CAD models from tissue imaging datasets.

Spiral tubule geometries were created in Fusion 360 and converted to ablation-compatible .mdb files as described above. The 3D curvature of spiral tubule geometries was designed to be in the physiologic curvature range of reconstructed mouse proximal tubules (Figure 2). To calculate the 3D curvature of reconstructed mouse proximal tubules, we employed a skeletonization and cubic spline interpolation approach from previous literature [14], [17]. First, a binary mask of the fully processed mouse proximal tubule was generated using 3D Slicer followed by skeletonization in FIJI. Skeleton coordinates were then imported into Matlab and cubic spline interpolation was used to generate new centerline points at 0.1μm intervals along the curve length. Curvature (κ) was then determined by computing the vector magnitude of the interpolated curve's second derivative at the resampled points:

$$\kappa = |r''(s)|$$

Where s denotes arc length and the interpolated curves have the form $r(s) = (x(s), y(s), x(s))$.

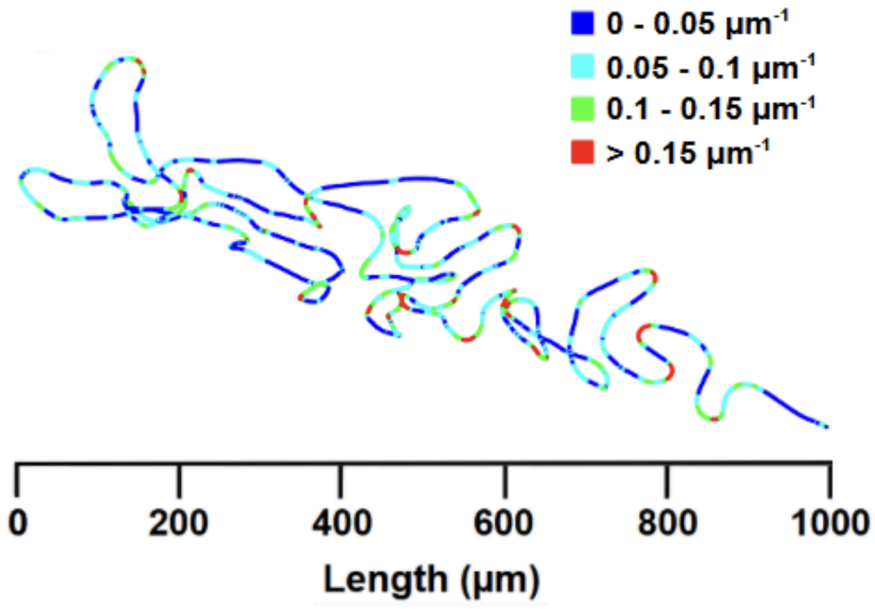

Figure 2: Calculated 3D curvature values along a mouse proximal tubule skeleton.

2.2 | Collagen microfluidic platform fabrication

Collagen hydrogels were selected due to their cell-remodelable properties, optical compatibility with multiphoton ablation, and widespread use as extracellular matrix mimics in vascular and renal tissue engineering. Collagen microfluidic devices were fabricated using a custom acrylic housing device and collagen isolated from rat tails. First, the acrylic housing devices were sterilized with a bleach solution and washed thoroughly with autoclaved de-ionized water. The inside chamber of the acrylic housing was treated with plasma and coated with 1% polyethyleneimine for 10 minutes. The polyethyleneimine was then aspirated and replaced with a 0.1% solution of glutaraldehyde for 20 minutes. The acrylic jigs were then washed thoroughly with autoclaved de-ionized water. In preparation for device fabrication, patterned PDMS stamps were created with a silicon wafer mold containing the desired geometry for the pre-patterned microchannel network. To fabricate collagen microchannels with soft lithography, a 10 mg/mL collagen solution was prepared and injected between the inside chambers of the acrylic housing and patterned PDMS stamps. The device and collagen were then left in the incubator for 1 hour to gel. PDMS stamps were then carefully removed and devices were closed with autoclaved screws. Assembled devices were left in the incubator overnight prior to laser ablation. Two photon ablation was performed through the glass coverslip at the bottom of each device.

A 2.5 W titanium-sapphire laser (Mai Tai HP, Newport) with a pulse duration of < 100 fs and repetition rate of 80 Mhz attached to a multiphoton microscope (FV1000, Olympus) and focused through a 25×1.05 NA objective (XLPlan N, Olympus) was used for laser ablation. Dwell time 2 µs per scan and λ = 800 nm were used, with pixel size set to 497×497 nm. Maximum power exiting the objective was 244 mW at 800 nm. Laser ablation of the glomerulus capillary network

was completed in ~90 minutes and ablation of the proximal tubule segment was completed in ~45 minutes.

2.3 | Cell culture and seeding

For cell isolation, human kidney cortical biopsies were obtained from a local biorepository (NWBioTrust). Kidney specimens were finely minced, treated with collagenase and placed in a shaker incubator at 37℃ for 30 minutes. The cell suspension was allowed to settle, and the supernatant was transferred to a tube containing 5 mL of horse serum. This solution was then mixed and centrifuged for 7 minutes at 1000 rpm. After centrifugation, the cells were plated and cultured using epithelial media. Cells were sorted into EPCAM-positive (epithelial) and EPCAM-negative (endothelial) populations. EPCAM-positive cells were plated or stored for hPTEC experiments. Primary isolated hPTECs were cultured in DMEM F-12 no glucose media supplemented with 0.1% D-glucose, 1% Antibiotic-Antimycotic, 1% Insulin-Transferrin-Selenium, and 0.1% Hydrocortisone. HUVECs were cultured in endothelial growth media (EGM). All hPTECsfor experimentation were used between passages 0 and 4.

After laser ablation, proximal tubule microchannel models were seeded with a hPTEC cell suspension of 10-14 x 10^6 cells/mL. A 10 µL volume of this cell suspension was injected into two device inlets with a gel-loading pipette to create flow across ablated microchannels. Immediately after this, 5 µL of growth media was added to the remaining outlet holes to reduce flow. Seeded devices were left in the incubator overnight to allow for complete hPTEC adherence prior to media changes. Devices culturing hPTECs were replenished with growth media every 24 hours and flow was minimized by injecting 200 µL of media into all reservoirs. To seed glomerular structures, a HUVEC cell suspension of 7 x 10^6 cells/mL was perfused

through pre-patterned collagen microchannels after glomerular ablation. The extensions added to the glomerular arterioles were purposely designed to leave a ~65 μm gap in between pre-patterned channels and the ablated glomeruli. HUVECs were allowed to settle and proliferate for 24-48 hours before a second ablation was conducted to connect the pre-patterned microchannels to the glomerular structures. HUVECs were then allowed to proliferate and migrate into the glomerular structures for 5 days.

2.4 | Immunocytochemistry (ICC)

For immunofluorescent staining, microvessels were fixed with 4% paraformaldehyde for 20 minutes by using gravity-driven flow across ablated microchannels. Microvessels were then washed with PBS three times for 10 minutes/wash. Blocking and permeabilization of microvessels was performed for 1 hour with a blocking buffer containing 2% bovine serum albumin and 0.1% Triton-X 100. Primary antibodies were then diluted in blocking buffer and perfused through the microvessels overnight. Microvessels were washed again with PBS three times for 10 minutes/wash. Secondary antibodies were diluted in blocking buffer and perfused through the microvessels for 1 hour (Table 1). Lastly, microvessels were washed a final time with PBS three times for 10 minutes/wash prior to fluorescence imaging.

Antibody or Stain	**Manufacturer**	**Catalog #**	**Species**	**Concentration**
LTL	Vector Labs	FL-1321	N/A	1:100
E-Cadherin	Cell Signalling Tech	3195	Rabbit anti-human	1:100
ZO-1	Invitrogen	33-9100	Mouse anti-human	1:500
Hoechst (Nuclei)	Thermo Fisher	H1399	N/A	1:200
Actin	Invitrogen	A12380	N/A	1:100
Na/K ATPase	Abcam	ab76020	Rabbit anti-human	1:100

Table 1: Immunostaining reagents for engineered glomerulus and tubule staining.

2.5 | Histology

After immunostaining, OCT solution was perfused through microvessels for 2 days with gravity driven flow. Following this, microvessels were disassembled and glass coverslip was removed from the top jig. The top jigs containing the microchannel network were then placed in a -80 ℃ freezer overnight. The top jigs were subsequently moved to a -20 ℃ freezer for 1 hour and the frozen collagen gel was carefully removed using a scalpel. The isolated collagen gels were allowed to equilibrate in OCT solution overnight. After this, OCT blocks containing the isolated collagen were labelled to indicate the direction of ablated microchannels and frozen using chilled

ethanol with dry ice. Prior to cryosectioning, gelatin-coated slides were prepared by immersing glass microscopy slides in a solution of chromium 3 sulfate dodecahydrate and porcine gelatin. The frozen OCT blocks were trimmed and mounted with the ablated microchannels perpendicular to the cryostat blade. The blocks were then sectioned at a thickness of 10 μm.

2.6 | Imaging and Quantification

Automated thresholding and counting of nuclei was performed in FIJI to determine the number of PTECs growing in microchannels. To calculate cell density, the number of PTECs counted per microchannel was divided by the internal surface area of each microchannel lumen ($SA = 2\pi rh$) where r represents the ablated channel radius and h represents the ablated channel length. To calculate a percent change in lumen expansion, the diameter at the center of each microchannel was measured and divided by the original microchannel diameter prior to cell seeding. For cell height analysis, individual images of microchannel cryosections were thresholded and a binary mask was produced covering the extent of the tubule wall. To quantify cell height, the local thickness plugin in FIJI was used on the binary masks and an average thickness value was calculated.

2.7 | Statistical Analysis

Statistical analysis was performed using GraphPad Prism. Differences between groups of microchannel diameters were assessed using a one-way ANOVA with Tukey's post hoc test. Statistical significance was defined as $p < 0.05$. Data for different diameter microchannels was taken from at least 2 separate microvessel devices.

3 | Results

3.1 | Fabrication of Anatomical Glomerulus and Proximal Tubule Models

To evaluate the ability of multiphoton ablation to generate anatomically organized nephron microstructures, we fabricated glomerulus and proximal tubule reconstructed models within collagen microfluidic platforms. First, we prepared a collagen hydrogel inside of an acrylic chip that could be imaged with a two-photon microscope via a glass coverslip viewing window. This system also contained a pre-patterned microchannel system connected to fluid reservoirs for the induction of flow within the system. A gap spanning 450 μm was left for laser ablation that would enable immediate connection of ablated structures to the pre-patterned microchannels (figure 3A). Using this platform, we successfully ablated a complete mouse glomerulus and showed a retention of capillary morphology under fluid flow with fluorescent bead perfusion (figure 3B, top). Similarly, we were also able to ablate a mouse proximal tubule segment and highlight its structure with fluorescent bead perfusion (figure 3B, bottom). To show the ability of ablated microstructures to support cell culture, human umbilical vein endothelial cells (HUVECs) from adjacent pre-patterned channels were allowed to migrate into ablated glomeruli and cultured for 5 days (figure 3C). Subsequent imaging showed HUVEC growth throughout the entire glomerular structure ranging from the arterioles to the tubular pole. Additionally, despite several days of cell growth, glomerular capillary structure was generally preserved, with only a few areas of significant collagen remodeling. In order to form an epithelium inside the ablated proximal tubule segment, we perfused a cell suspension of human proximal tubule epithelial cells (hPTECs) and incubated the device for 5 days (figure 3D). Analysis of the ablated proximal tubule segment after hPTEC culture showed that a robust epithelium could be formed throughout the entire structure and tubular morphology was well maintained.

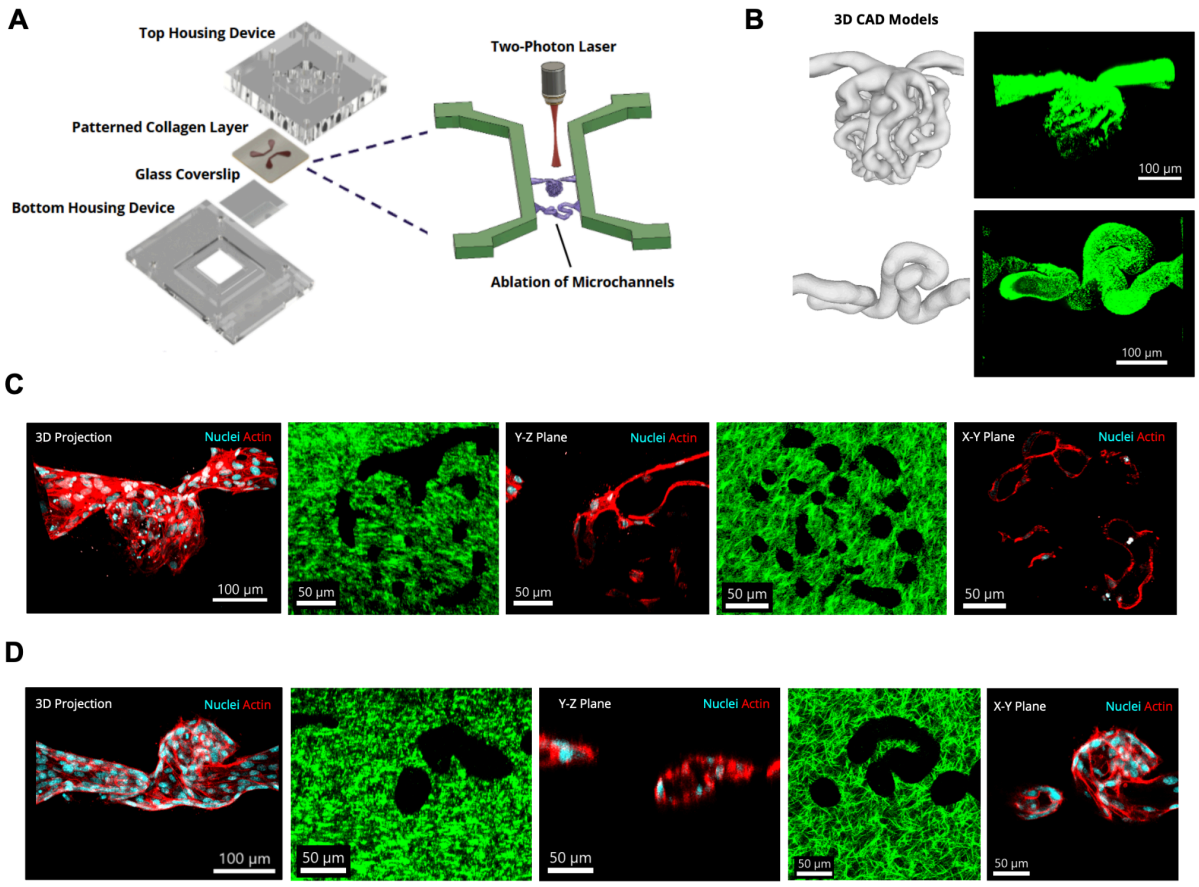

Figure 3: Fabrication of anatomical nephron microstructures within a microfluidic device. (A) Device assembly and microchannel creation with multiphoton ablation. (B) Perfusion of a mouse glomerulus structure (top) and mouse proximal tubule segment (bottom). (C) Cellularization of mouse glomerulus. Engineered glomerulus visualized as a 3D projection (left) and in matching cross sections of collagen matrix and HUVECs. (D) Cellularization of mouse proximal tubule segment. Engineered tubule visualized as a 3D projection (left) and in matching cross sections of collagen matrix and hPTECs.

3.2 | Proximal Tubule Epithelium Characterization in Pre-patterned and Ablated Microchannels

Historically, in vitro models have been unable to combine the small luminal diameter (<60 µm) of the proximal tubule and 3D curvature [6], [7], [8], [9]. To address this limitation, we sought

to use laser ablation to fabricate a cell based model of the proximal tubule that combined physiologic diameter and curvature. To confirm the ability of our collagen microchannel platform to sustain polarized proximal tubule epithelia, we cultured hPTECs within larger, non-curved microchannels for 2 weeks and visualized key markers of epithelial junction formation and polarization with immunofluorescence staining. Within these pre-patterned microchannels, hPTECs form a completely patent epithelium (Figure 4A) and display cortical actin localization that is characteristic of polarized tubular epithelia (Figure 4B). Moreover, hPTECs displayed apical grouping of LTL which is indicative of brush border maturation (Figure 3C). Additionally, we observed robust staining of E-Cadherin and ZO-1 throughout the hPTEC epithelium which suggests proper cell-cell adhesion and tight junction formation (Figure 4D-E). Lastly, hPTECs showed appropriate basolateral localization of the major ion transporter Na/K ATPase, further confirming functional polarization of the epithelium (Figure 4F). These results suggest that our microchannel platform and collagen hydrogel matrix is well suited for the culture of hPTECs and proximal tubule modeling.

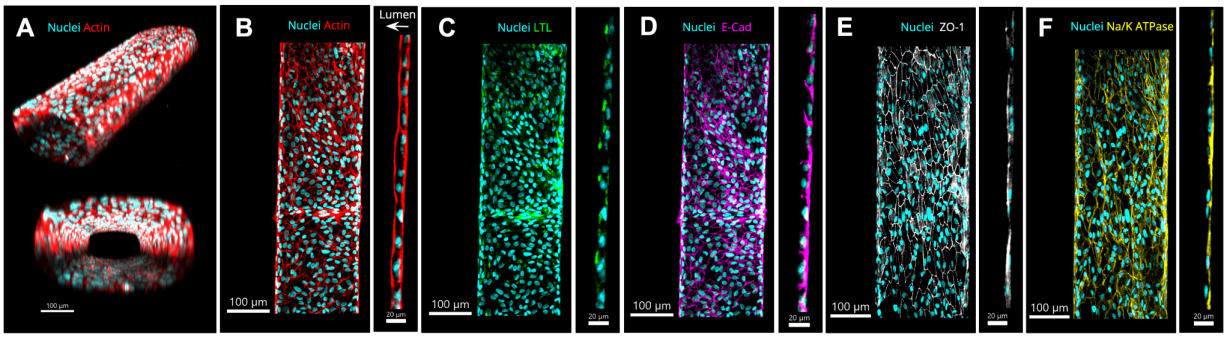

Figure 4: PTEC Growth and Epithelium formation in Collagen Microchannel Networks. (A) 3D view of PTECs forming patent epithelia in pre-patterned microchannels. (B-F) Confocal images of PTECs within pre-patterned microchannels, visualized as a 3D projection and cross sectional view. PTECs display robust expression of cortical actin (B), apical LTL (C), lateral E-Cadherin (D), apical ZO-1 (E), and basolateral Na/K ATPase (F).

Next, we used laser ablation to create a spiral microchannel of constant curvature 0.012 μm^{-1} with a diameter of 60 µm. We then perfused hPTECs through this spiral microchannel and cultured the devices for 2 weeks before analyzing epithelium formation with immunofluorescence staining. After 2 weeks, hPTECs form a complete epithelium throughout the spiral microchannel and retain its diameter and 3D structure (Figure 5A). Spiral tubule models also show cortical actin organization (Figure 5B), LTL grouping (Figure 5C) and junctional E-Cadherin organization (Figure 5D). Cross sectional visualization of the spiral tubules revealed development of apical LTL localization and lateral E-Cadherin in several areas of the engineered tubules (Figure 5E-F). Overall, these results show that laser ablation can be used to create in vitro proximal tubule models with the fundamental structural properties of the native proximal tubule.

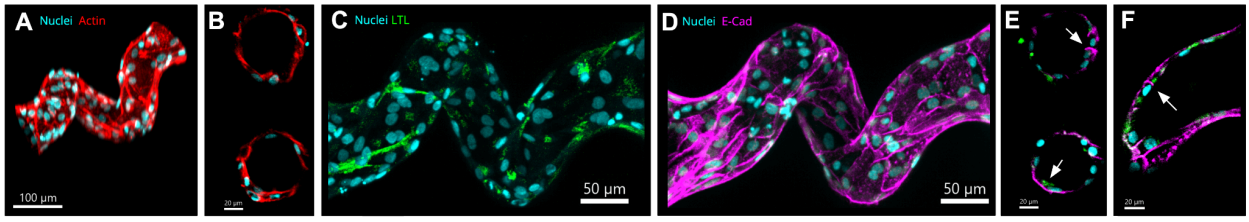

Figure 5: PTEC Growth and Epithelium formation in Spiral Microchannels. (A) 3D view of engineered spiral tubule. (B) Cross sectional view of spiral tubule shows PTECs forming a patent epithelium with cortical actin organization. (C-D) 3D projections of spiral tubules showing LTL and E-Cadherin expression throughout the epithelium. (E-F) Cross sectional view of spiral tubules showing apical LTL localization and lateral E-Cadherin.

3.3 | Proximal Tubule Epithelial Cell Behaviour in Microchannel Diameters below 100 µm

Epithelial cells in the proximal tubule are spatially constrained and grow on a distinctly curved surface due to the small diameter of the proximal tubule. Microfluidic models of the proximal

tubule with larger diameters cannot accurately replicate the tubular microenvironment in which the luminal curvature experienced by cells is directly related to the channel diameter (Figure 6A). Previous studies have investigated the influence of luminal curvature on renal epithelial cell phenotype and behavior, but have relied on non-degradable, synthetic materials and non-human cell types for model fabrication [18], [19]. To better understand renal epithelial cell behavior in tubular compartments with anatomical diameter, we analyzed cell morphology and polarization in hPTECs cultured inside collagen microchannels with diameters ranging from 40-100 μm. After 2 weeks of culture hPTECs formed complete patent epithelia in all microchannel diameters with consistent staining of proximal tubule markers E-Cadherin and LTL (Figure 6B-D). Despite the higher physical constraint present in smaller diameter microchannels (40-60 μm), hPTEC density was not significantly different across microchannel diameters (Figure 6E). Similarly, the luminal enlargement arising from PTEC remodelling of surrounding collagen was not different across microchannel diameters (Figure 6F). Imaging and analysis of cryosections from all microchannel diameters showed that cell height was consistent across 40-100 μm diameters. Interestingly, when compared to pre-patterned microchannels with diameters above 200 μm and hPTEC cultures between 1-2 weeks, hPTEC height was found to be significantly reduced in ablated microchannels with diameters of 100 μm or below (Figure 6G). These results suggest that fabrication of engineered tubules at physiologic diameters below 100 μm reduces the formation of hPTEC columnar morphology.

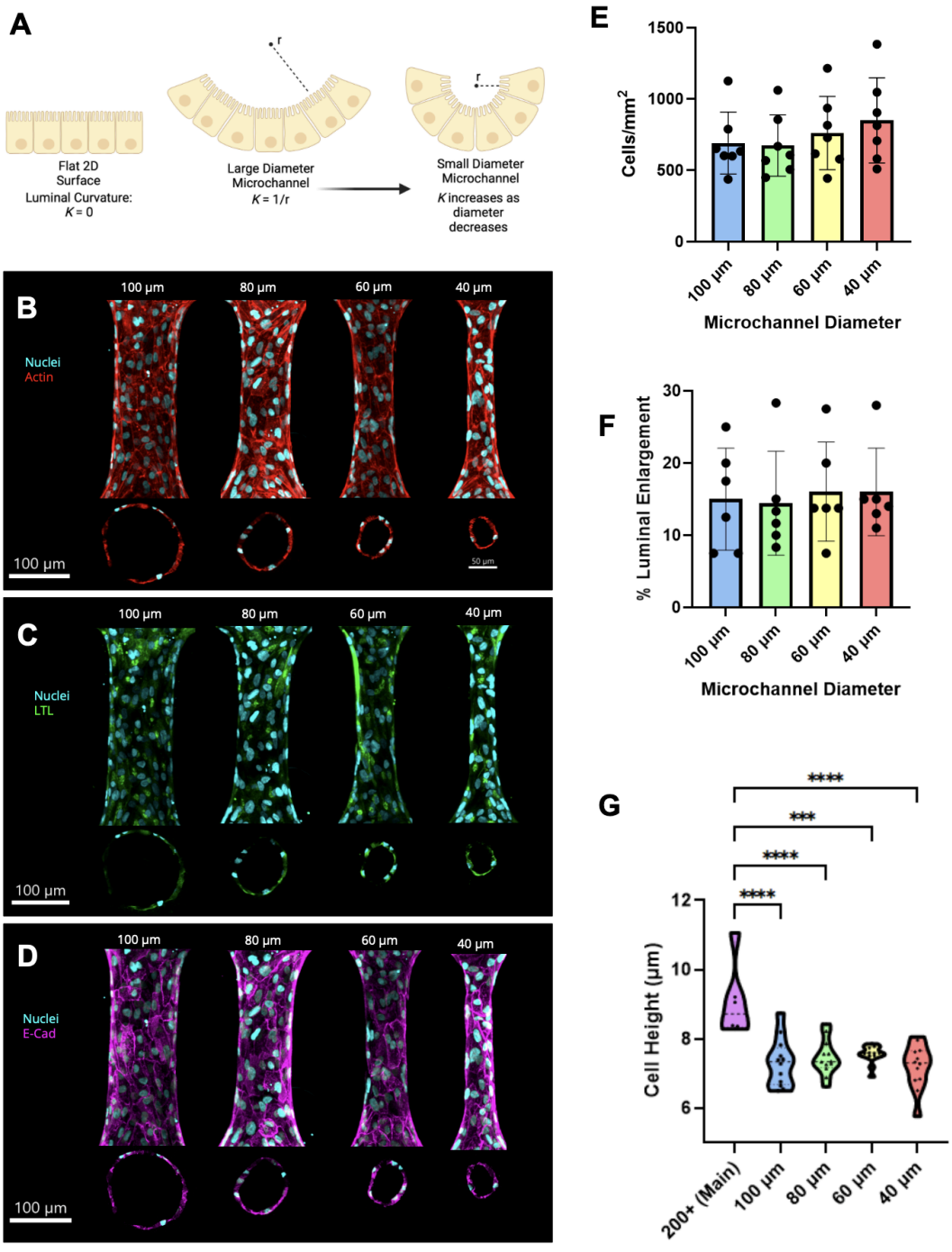

Figure 6: PTEC Growth and Polarization in varying Microchannel Diameters. (A) Luminal curvature is dependent on microchannel diameter (B-D) Z-stack projections and sectioned slices of PTECs cultured in microchannels ranging from 40-100 µm in diameter. (E) Number of PTECs growing in varying microchannel diameters. (F) PTEC height quantification in varying microchannel diameters.

4 | Discussion

In this study, we showed that laser ablation can be used for the subtractive manufacturing of renal nephron microstructures at anatomical scales below 100 μm. We show the flexibility of this approach by laser ablating both a full glomerulus structure and proximal tubule segment, whose structure was determined with different imaging modalities. Furthermore, we highlight the utility of laser ablation for tissue engineering applications by showing that ablated nephron microstructures support endothelial and epithelial cell culture. We used laser ablation to address key limitations in proximal tubule in vitro modeling by creating an engineered proximal tubule with both anatomical diameter and curvature. Lastly, we used laser ablation to investigate the behavior of hPTECs in collagen microchannels with physiologic tubule diameters and observed that luminal confinement in sub 100 μm microchannels limited hPTEC height.

The multiphoton ablation technique described in this work can theoretically fabricate any structure represented as a CAD object. However, the size and complexity of structures may present a limitation due to the need for increased microscope scanning time. For example, the amount of branching present in a structure will increase the areas to scan for each cross sectional slice, regardless of the total volume occupied by a structure. Because of this, ablation of glomerular microstructures required ~90 minutes of microscope scanning time whereas proximal tubule microstructures required ~45 minutes of scanning.

Although laser ablation was able to precisely reproduce both glomerular and proximal tubule segments with high accuracy, cell seeding of these structures was less accurate. Areas were present in which cells did not infiltrate ablated microstructures or engaged in collagen matrix remodelling. These issues may be resolved with further optimization of cell seeding density, increased culture time for more extensive cell infiltration, or higher concentrations of collagen

hydrogels to reduce remodelling. Prolonged culture of hPTECs in pre-patterned microchannels and spiral microchannels yielded epithelium formation with characteristic features of renal epithelial polarization. However, when compared to in vivo, hPTECs cultured within our system still display a limited phenotype. This may be attributed to issues with primary human renal epithelial cells which quickly lose phenotypic properties with expansion [20]. A possible future alternative may be organoid-derived proximal tubular epithelial cells which have been used to populate in vitro tubular models and display strong phenotypic attributes [21].

Due to the difficulty in fabricating tubular tissues with small diameters, the influence of the tubular microenvironment on renal epithelial cells remains largely unknown. In particular, the response of renal epithelial cells to the luminal curvature inside of the proximal tubule and physical constraint of growing in a compact tube is unclear. Xi et al. sought to answer these questions by culturing canine renal epithelial cells (MDCK) in polydimethylsiloxane (PDMS) microchannels of varying diameters [19]. MDCKs in this study showed increased cell height in channels below 100 μm in diameter when compared to 2D culture. However, the behavior of human renal epithelial cells undergoing tubular confinement remains unclear. To address this, Yu et al. cultured immortalized human cells on curved or flat PDMS surfaces and analyzed cell phenotype [18]. In this previous study, HK-2 cells showed increased cell height when cultured on curved surfaces when compared to flat surfaces. However, the genetic modification of HK-2 cells [22] and usage of synthetic non-degradable materials remain as key limitations. Our results indicate that within collagen microchannels, hPTECs develop a height comparable to previous models. However, we observed a decrease in hPTEC height at smaller channel diameters which is the opposite of what has been reported in previous studies.

Bibliography

[1] M. Zhou *et al.*, “Development of a Functional Glomerulus at the Organ Level on a Chip to Mimic Hypertensive Nephropathy,” *Sci. Rep.*, vol. 6, no. 1, p. 31771, Aug. 2016, doi: 10.1038/srep31771.

[2] M. G. Valverde *et al.*, “Biomimetic models of the glomerulus,” *Nat. Rev. Nephrol.*, vol. 18, no. 4, pp. 241–257, Apr. 2022, doi: 10.1038/s41581-021-00528-x.

[3] L. Wang, T. Tao, W. Su, H. Yu, Y. Yu, and J. Qin, “A disease model of diabetic nephropathy in a glomerulus-on-a-chip microdevice,” *Lab. Chip*, vol. 17, no. 10, pp. 1749–1760, May 2017, doi: 10.1039/C7LC00134G.

[4] S. Sundaram *et al.*, “Sacrificial capillary pumps to engineer multiscalar biological forms,” *Nature*, vol. 636, no. 8042, pp. 361–367, Dec. 2024, doi: 10.1038/s41586-024-08175-5.

[5] E. J. Weber *et al.*, “Development of a microphysiological model of human kidney proximal tubule function,” *Kidney Int.*, vol. 90, no. 3, pp. 627–637, Sep. 2016, doi: 10.1016/j.kint.2016.06.011.

[6] K. A. Homan *et al.*, “Bioprinting of 3D Convoluted Renal Proximal Tubules on Perfusable Chips,” *Sci. Rep.*, vol. 6, no. 1, p. 34845, Oct. 2016, doi: 10.1038/srep34845.

[7] A. M. van Genderen *et al.*, “Co-axial printing of convoluted proximal tubule for kidney disease modeling,” *Biofabrication*, vol. 14, no. 4, p. 044102, Jul. 2022, doi: 10.1088/1758-5090/ac7895.

[8] N. K. Singh *et al.*, “Three-dimensional cell-printing of advanced renal tubular tissue analogue,” *Biomaterials*, vol. 232, p. 119734, Feb. 2020, doi: 10.1016/j.biomaterials.2019.119734.

[9] K. Tröndle *et al.*, “Scalable fabrication of renal spheroids and nephron-like tubules by bioprinting and controlled self-assembly of epithelial cells,” *Biofabrication*, vol. 13, no. 3, p. 035019, Apr. 2021, doi: 10.1088/1758-5090/abe185.

[10] G. Kiranmai *et al.*, “Recent trends in the development of in vitro 3D kidney models,” *Biofabrication*, vol. 17, no. 2, p. 022010, Mar. 2025, doi: 10.1088/1758-5090/adb999.

[11] O. Ilina, G.-J. Bakker, A. Vasaturo, R. M. Hoffman, and P. Friedl, “Two-photon laser-generated microtracks in 3D collagen lattices: principles of MMP-dependent and -independent collective cancer cell invasion,” *Phys. Biol.*, vol. 8, no. 1, p. 015010, Feb. 2011, doi: 10.1088/1478-3975/8/1/015010.

[12] S. G. Rayner *et al.*, “Multiphoton-Guided Creation of Complex Organ-Specific Microvasculature,” *Adv. Healthc. Mater.*, vol. 10, no. 10, p. 2100031, 2021, doi: 10.1002/adhm.202100031.

[13] C. Arakawa *et al.*, “Biophysical and biomolecular interactions of malaria-infected erythrocytes in engineered human capillaries,” *Sci. Adv.*, vol. 6, no. 3, p. eaay7243, Jan. 2020, doi: 10.1126/sciadv.aay7243.

[14] D. A. Kim, A. Armenta, J. C. Vaughan, M. Terasaki, J. Himmelfarb, and Y. Zheng, “Hemodynamic simulation and in vitro modeling of three-dimensional glomeruli at anatomical scale,” *Phys. Fluids*, vol. 37, no. 5, p. 051907, May 2025, doi: 10.1063/5.0264128.

[15] M. Terasaki, J. C. Brunson, and J. Sardi, “Analysis of the three dimensional structure of the kidney glomerulus capillary network,” *Sci. Rep.*, vol. 10, no. 1, p. 20334, Nov. 2020, doi: 10.1038/s41598-020-77211-x.

[16] M. Y. Lee *et al.*, “Fluorescent labeling of abundant reactive entities (FLARE) for cleared-tissue and super-resolution microscopy,” *Nat. Protoc.*, vol. 17, no. 3, pp. 819–846, Mar. 2022, doi: 10.1038/s41596-021-00667-2.

[17] S. Lorthois, F. Lauwers, and F. Cassot, “Tortuosity and other vessel attributes for arterioles and venules of the human cerebral cortex,” *Microvasc. Res.*, vol. 91, pp. 99–109, Jan. 2014, doi: 10.1016/j.mvr.2013.11.003.

[18] S.-M. Yu *et al.*, “Substrate curvature affects the shape, orientation, and polarization of renal epithelial cells,” *Acta Biomater.*, vol. 77, pp. 311–321, Sep. 2018, doi: 10.1016/j.actbio.2018.07.019.

[19] W. Xi, S. Sonam, T. Beng Saw, B. Ladoux, and C. Teck Lim, “Emergent patterns of collective cell migration under tubular confinement,” *Nat. Commun.*, vol. 8, no. 1, p. 1517, Nov. 2017, doi: 10.1038/s41467-017-01390-x.

[20] O. C. Klatt *et al.*, “Human and rat renal proximal tubule in vitro models for ADME applications,” *Arch. Toxicol.*, vol. 99, no. 5, pp. 1613–1641, May 2025, doi: 10.1007/s00204-025-03987-4.

[21] J. O. Aceves *et al.*, “3D proximal tubule-on-chip model derived from kidney organoids with improved drug uptake,” *Sci. Rep.*, vol. 12, no. 1, p. 14997, Sep. 2022, doi: 10.1038/s41598-022-19293-3.

[22] T. Petreski, L. Varda, L. Gradišnik, U. Maver, and S. Bevc, “Renal Proximal Tubular Epithelial Cells: From Harvesting to Use in Studies,” *Nephron*, vol. 147, no. 11, pp. 650–654, Jul. 2023, doi: 10.1159/000531291.